ICAS 2021 SHANG HAI
International Council of the Aeronautical Sciences
32nd Congress of the International Council of the Aeronautical Sciences
September 6-10, 2021 Pudong Shangri-La, Shanghai, China

PARETO FRONT EXPLORATION USING MANIFOLD RECONSTRUCTION APPROACH FOR ROTORCRAFT AIRFOILS DESIGN

Song Chao, Li Weibin, Zhou Zhu, Liu Hongyang, Luo Xiao

Computational Aerodynamics Institute, China Aerodynamics Research and Development Center, Mianyang, 621000, China

Abstract

The rotor airfoils for the helicopter experience dramatically different conditions within a single rotation cycle and many objectives and constrains must be considered during the design and optimization. A manifold learning approach for the Pareto front exploration has been developed in this paper. The manifold structure of Pareto front of a multi-objective problem is explored and reconstructed using the manifold learning method. The method is validated by analytical problems, and a three-objectives design problem of the rotor airfoil. Enhanced with the approach, the evolutionary optimization converges more rapidly, and the diversity and uniformity of the optimal Pareto are improved evidently. The multi-objective optimization enhanced with manifold learning shows promising capability in practical application.

Keywords: multi-objective; manifold; rotor airfoil; aerodynamic; optimization

1. Introduction

The aerodynamic characteristics of airfoils are critical for the improvement of helicopter blade performance. However, the design of airfoils for the helicopter is full of challenges, because airfoils experience dramatically different conditions within a single rotation cycle. For the forward flight condition, a regime of transonic flow exits around the tip of the forward blade, leading to a shock wave and boundary layer intersection. The retreating blade must generate enough lift at the same time to maintain helicopter roll stability. Besides, high lift coefficients at low and moderate Ma numbers are requested, at all fight conditions. A small pitching moment also needs be achieved for helicopter manipulability. Therefore, the design of rotor airfoils is a multi-objective problem with strong multi-constraints.

Wang[1] carried out optimization on SC1095 airfoil aimed at improving the characteristics of airfoil under dynamic stall conditions. Hager[2] developed a two design-points design method for airfoils in the rotational transonic flows. Jones[3] designed rotorcraft airfoils that address aerodynamic and aeroacoustic concerns using a parallel genetic algorithm. Massaro and Benini[4] proposed a multi-objective approach for rotor airfoil optimization using surrogate-assisted memetic algorithm. However, in most of the researches, only a part of characteristics of rotor airfoils are considered resulted in partial performance improvement. If all the design objectives are considered, a high-dimensional multi-objective problem will be resulted in and the optimization algorithms will encounter a bottleneck[5], and the Pareto front is hard to be found. For this reason, little research has aimed at the improvement for more than three objectives for rotor airfoils. Zhao[6] proposed a principle component analysis (PCA) dimensionality reduction method, and a high dimensional problem with six-objective is translated into a bi-objective problem.

In most of the multi-objective optimizations, the regularity that the Pareto set of a continuous m-objectives problem is a piecewise continuous (m-1) dimensional manifold is always neglected. The regularity of the population distribution is formed gradually with the population evolutionary. Yet, few methods exist that take advantage of the manifold information of the Pareto front to aid the multi-objective optimization. Daskilewicz[7] described a process for parameterizing Pareto front employing self-organizing maps. Yang[8] proposed a multi-objective evolutionary algorithm combined with the locally linear embedding (LLE), which is a representative manifold learning method.

In this paper, a novel algorithm for multi-objective optimization enhanced with a manifold reconstruction method is proposed. The algorithm rebuilds the distribution of the Pareto front in the manifold space using the manifold learning method. Therefore, the high dimensional design space is mapped to the (m-1) dimensional space. Then a child population is generated in the manifold space, and the optimization algorithm is enhanced by the manifold information. The proposed method, based Manifold Reconstruction based Estimation of Distribution Algorithms (MR-EDA) is introduced in detail in section 2, and the algorithm is validated by analytical problems in section 3. Then the algorithm is applied to the rotor airfoil optimization problems with 3 objectives and the results are analysis in section 4. At last, the conclusion is shown in section 5.

2. Manifold Reconstruction Based Estimation of Distribution Algorithms

2.1 Manifold Reconstruction

Almost the manifold learning approaches can map the data in the high-dimensional space to a low-dimensional manifold space. However, analytic expression is not able to provide for the mapping process. For a specific aerodynamic design problem, although we can map the sample points in the design space to a manifold space, however, the mapped points in the low-dimensional manifold has no specific physical meaning. Thus, the manifold information is hard to utilize. For example, we cannot obtain a sample point in the design space corresponding to any specified points in the manifold space, and there has no way to solve aerodynamic forces.

A manifold reconstruction method must be used to employing the manifold information during the optimization process. Set $\mathbf{S}^k$ is a k-dimensional manifold, which is embedding is a n-dimensional space $\mathbf{D}^n$, where $k << n$. $\{\mathbf{x}_i\}\big|_{i=1}^N$ is N sample points in $\mathbf{D}^n$, and $\{\mathbf{y}_i\}\big|_{i=1}^N$ is N sample points in $\mathbf{S}^k$. The relation between $\mathbf{x},\mathbf{y}$ is $\mathbf{y} = f(\mathbf{x}), \mathbf{x} = \mathrm{g}(\mathbf{y})$. According to the Taylor expansion theorem, any point $\mathbf{y}$ in the neighborhood of $\mathbf{y}_i$ can be expressed as:

$$\mathbf{x} = \mathrm{g}(\mathbf{y}) = \mathbf{x}_i + J(\mathbf{y}_i)(\mathbf{y} - \mathbf{y}_i) + \mathrm{R}(\mathbf{y}, \mathbf{y}_i) \tag{1}$$

where $J(\mathbf{y}_i)$ is the Jacobian matrix of $\mathrm{g}(\mathbf{y})$ at the point $\mathbf{y}_i$, and the $\mathrm{R}(\mathbf{y}, \mathbf{y}_i)$ is the remainder term. Ignoring the remainder term and assume $\mathbf{x}_i$ has z points in the neighborhood, we have the equations:

$$\begin{aligned} &\mathbf{X}_i \approx J(\mathbf{y}_i)\mathbf{Y}_i, \\ &\mathbf{X}_i = (\mathbf{x}_{i,1} - \mathbf{x}_i, \ldots, \mathbf{x}_{i,z} - \mathbf{x}_i), \\ &\mathbf{Y}_i = (\mathbf{y}_{i,1} - \mathbf{y}_i, \ldots, \mathbf{y}_{i,z} - \mathbf{y}_i) \end{aligned} \tag{2}$$

$$J(\mathbf{y}_i) \approx (\mathbf{X}_i \mathbf{Y}_i^{\mathrm{T}})(\mathbf{Y}_i \mathbf{Y}_i^{\mathrm{T}})^{-1} \tag{3}$$

Now we obtain the Jacobian matrix $J(\mathbf{y}_i)$ at the point $\mathbf{y}_i$.

For any point $\mathbf{y}$ in the manifold space $\mathbf{S}^k$, the $\mathbf{x}$ in the high-dimensional space $\mathbf{D}^n$ can be solved by the steps:

1, Find the point $\mathbf{y}_s$ in $\{\mathbf{y}_i\}\big|_{i=1}^N$,which is the nearest to the point $\mathbf{y}$;

2, Find the $\mathbf{x}_s$ in high-dimensional $\mathbf{D}^n$ corresponding to $\mathbf{y}_s$, and the neighborhood points $\mathbf{x}_{s,1}, \mathbf{x}_{s,2}, \ldots, \mathbf{x}_{s,z}$ of $\mathbf{x}_s$. Then the embedding points $\mathbf{y}_{s,1}, \mathbf{y}_{s,2}, \ldots, \mathbf{y}_{s,z}$ of the neighborhood points in $\mathbf{S}^k$ can be obtained;

3, Build the matrix $\mathbf{X}_s = (\mathbf{x}_{s,1} - \mathbf{x}_s, \ldots, \mathbf{x}_{s,z} - \mathbf{x}_s)$ and matrix $\mathbf{Y}_s = (\mathbf{y}_{s,1} - \mathbf{y}_s, \ldots, \mathbf{y}_{s,z} - \mathbf{y}_s)$, then the matrix $\mathbf{Q}_s = (\mathbf{X}_s \mathbf{Y}_s^{\mathrm{T}})(\mathbf{Y}_s \mathbf{Y}_s^{\mathrm{T}})^G$;

4, At last, the embedding pointed of point $\mathbf{y}$ in $\mathbf{D}^n$ is $\mathbf{x} \approx \mathbf{x}_s + \mathbf{Q}_s(\mathbf{y} - \mathbf{y}_s)$.

2.2 MR-EDA framework

Estimation of distribution algorithms (EDAs)[10~12] are a class of evolutionary algorithms. The key process in EDAs is the probabilistic models construction. Regularization techniques, which are widely used in statistics and machine learning[13], have been used in EDAs to obtain a robust prediction model. The proposed method adopts the manifold reconstruction for estimating a probability distribution model for the space of possible candidate solutions to the given problem. Compared with

the regularization techniques, the manifold reconstruction takes advantages of the manifold structure of the Pareto front. What's more, the evolutionary process has much more direct physical meaning. The flowchart of the MR-EDA is presented in Figure 1.

The basic steps of the MR-EDA are introduced as follow:

1. Generate an initial population **Pop**(0), and solve the objective function **F**(**x**);
2. Obtain a non-dominated solution set **Q**(t)by sorting the objectives, where t is the iteration step;
3. Assume **Q**(t) is a high dimensional manifold, and the **F**(**x**) is the low-dimension embedding manifold of **Q**(t). Using the approach in section 2.1, generate a promising distribution of solution set **P**(t);
4. Obtain a new population **Pop**(t) by merging the **Q**(t) and **P**(t), if the convergence condition is reached, the optimization process stops, else go to step 1 for iteration.

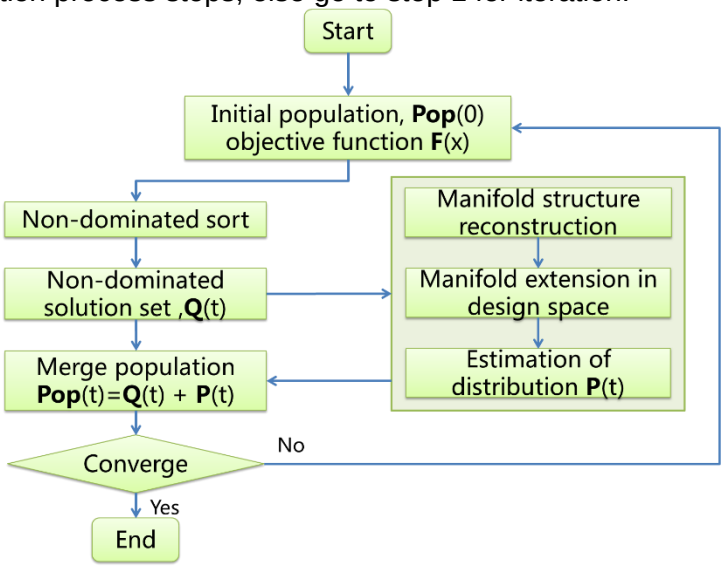

Figure 1 Flow chart for MR-EDA

3. Analytical Problems Validation

In order to validate the performance of the MR-EDA, here we give the results on analytical problems. The result will be compared with the NSGA-Ⅱ, a fast and elitist multi-objective genetic algorithm. The three test instances are from the ZDT test suit, and the definitions are presented in Table 1. The inverted generational distance (IGD)[9] is used for performance evaluation of the multi-objective optimization method. A small value of the IGD implied the good convergence of solutions to the Pareto front and their good distribution over the entire Pareto front. The IGD is defined as:

$$IGD(S^*,S)=\frac{\sum_{v\in S^*} d(v,S)}{|S^*|} \tag{4}$$

where the $d(v,S)$ is the minimum distance of the point v to the points in the Pareto set S, which is obtained by the optimization method. S^* is the true Pareto front and the $|S^*|$ is the points number in the set.

The number of design variables is 30 in the three test instances, and the number of population is 100. The optimization will be stopped when the maximum iteration step, 200 is reached. Especially for the NSGA-Ⅱ, the cross probability is 0.8 and the mutation probability is 0.3.

Figure 2 shows the optimal Pareto front obtained by the proposed method and the NSGA-Ⅱ for the ZDT1 test instance, and the true front is also presented in the figure. As it clearly indicated in the Figure 2, the optimal front obtained by the MR-EDA almost coincide with the true front, however, the optimal front after 200 iterations using the NSGA-Ⅱ is still not converged the true front. The IGD indicator could show a converge history of the iterations, as shown in Figure 3. The value of the IGD by the MR-EDA converges more rapidly than the NSGA-Ⅱ, and the former is close to zero after about 150 iterations.

For the ZDT2 test instance, the MR-EDA also shows the good ability of Pareto front exploration. As shown in Figure 4 and Figure 5, the MR-EDA can find the true front after about 110 iterations.

However, the NSGA-Ⅱ converges much slower.

The true front of the ZDT3 is piecewise continuous, as shown in Figure 6. Both the MR-EDA and NSGA-Ⅱ do not converge to the true front, but the convergence rate of MR-EDA is obviously improved, as presented in Figure 7.

This indicates that the convergence speed using the MR-EDA has been improved significantly, compared with the NSGA-Ⅱ. What's more, the population diversity and uniformity in the optimal Pareto front are also improved obviously. These results encourage the application of the proposed method to more complex problems. In the subsequent study, the MR-EDA will be applied to multi-objective optimization problems for rotor airfoils, and its prominent ability of the proposed method should be verified.

Table 1 Definitions of the test functions

Test instances	Definition	True Pareto front
ZDT1	$g(x)=1+9\sum_{i=2}^{m}x_i/(\mathrm{m}-1)$ $F_1(x)=x_1$ $F_2(x)=g(x)(1-\sqrt{x_1/g(x)}),\ x\in[0,1]$	$y=1-\sqrt{x_1}$
ZDT2	$g(x)=1+9\sum_{i=2}^{m}x_i/(\mathrm{m}-1)$ $F_1(x)=x_1$ $F_2(x)=g(x)(1-(\frac{x_1}{g(x)})^2),\ x\in[0,1]$	$y=1-x_1^2$
ZDT3	$g(x)=1+9\sum_{i=2}^{m}x_i/(\mathrm{m}-1)$ $F_1(x)=x_1$ $F_2(x)=g(x)(1-\sqrt{\frac{x_1}{g(x)}}-\frac{x_1}{g(x)}\sin(10\pi x_1)),\ x\in[0,1]$	$y=1-\sqrt{x_1}-x_1\sin(10\pi x)$

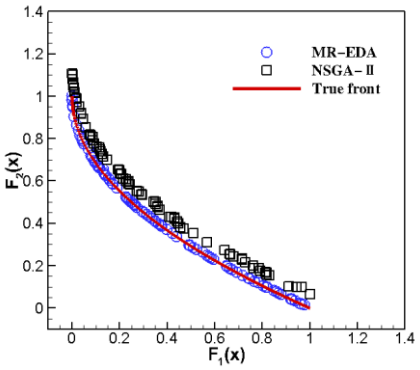

Figure 2 Optimal front of ZDT1 test case obtained by the NSGA-Ⅱ and MR-EDA

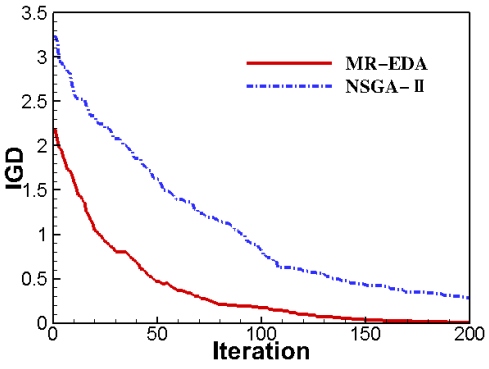

Figure 3 Convergence histories of IGD of ZDT1 test case using NSGA-Ⅱ and MR-EDA

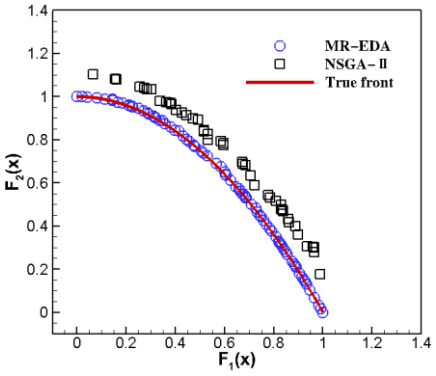

Figure 4 Optimal front of ZDT2 test case obtained by the NSGA-Ⅱ and MR-EDA

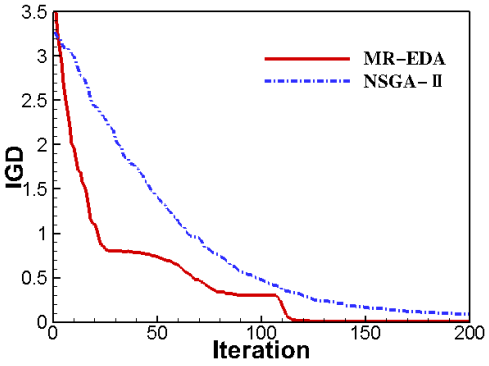

Figure 5 Convergence histories of IGD of ZDT2 test case using NSGA-Ⅱ and MR-EDA

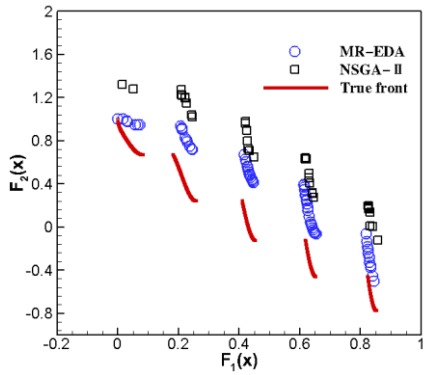

Figure 6 Optimal front of ZDT3 test case obtained by the NSGA-Ⅱ and MR-EDA

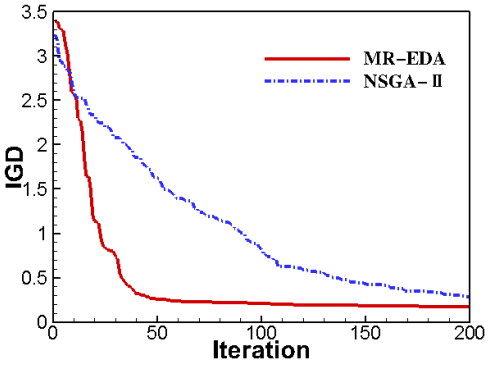

Figure 7 Convergence histories of IGD of ZDT3 test case using NSGA-Ⅱ and MR-EDA

4. Multi-objective Designs for OA209 Using MR-EDA

4.1 Multi-objective optimization problem definition

The OA209 airfoil, developed by ONERA, is chose for the baseline airfoil, as shown in the Figure 8. The airfoil has been parameterized by the CST, and the order of the upper and lower surfaces are both 6, thus 14 design variables are used for the airfoil design process.

Several basic performances should be considered for the rotor airfoil, such as the low drag level at hover flight condition, high maximum lift coefficient at maneuvering flight condition, low drag divergence Ma number, and low level moment coefficient at zero lift condition. Thus, the optimization problem for high performance rotor airfoil is defined as:

$$\begin{aligned}
&\text{Objective}\begin{cases}\min\ f_1 = C_D / C_{D1}^0\\ \min\ f_2 = -C_{L2} / C_{L2}^0\\ \min\ f_3 = [(C_{D3}-C_{D4})^2+(C_{D4}-C_{D5})^2]/(\Delta\text{Ma})^2/0.005\end{cases}\\
&\text{subject to } \hat{g}_i(\mathbf{x}) \le 0,\ i = 1\sim 7\\
&\quad A > A^0 \times 0.995\\
&\quad \left|(t-t^0)/t^0\right| \le 0.01\\
&\quad \mathbf{x}_l \le \mathbf{x} \le \mathbf{x}_u
\end{aligned} \tag{5}$$

where the sup script 0 indicate the baseline performance, A is the area of the airfoil, and t is the maximum thickness of the airfoil. In this optimization problem, 7 conditions are involved, as shown in Table 2. The first design objective is the minimum drag coefficient at $Ma = 0.6, C_L = 0.6$, and the lift coefficient is considered as a constraint. The second objective is the negative lift coefficient at $Ma = 0.4$ with the drag coefficient constrained. The last objective is the drag divergence Ma number, and the objective value is normalized by dividing 0.005 to close to 1. The moment coefficients at zero lift

condition are all considered as constraints, as presented in Table 2.

Table 2 Design points and constraints for the rotor airfoil

Flight condition	Objective	Design point	Constraint
Hover flight $Ma = 0.6$ $C_L = 0.6$	$C_D(\text{design}) \le \mathrm{C_D}(\text{OA 209})$	$Ma = 0.6$ $\mathrm{Re} = 4.8\times10^6$ $\alpha = 3.23^\circ$	$C_{L1} \ge C_{L1}^0$
Maneuvering flight $Ma = 0.4$ $C_L = C_{L\max}$	$C_{L\max}(\text{design}) \le \mathrm{C}_{L\max}(\text{OA 209})$	$Ma = 0.4$ $\mathrm{Re} = 3.2\times10^6$ $\alpha = 11.0^\circ$	$C_{D2} \le C_{D1}^0$
Forward flight $C_L = 0.0$	$Ma_{Dd0}(\text{design}) \ge Ma_{Dd0}(\text{OA 209})$ $\lvert C_{m0}\rvert \le 0.01$	$Ma = 0.76$ $\mathrm{Re} = 6.08\times10^6$ $\alpha = -0.9^\circ$	$C_{D3} \le C_{D3}^0$ $\lvert C_{m3}\rvert \le \lvert C_{m3}^0\rvert$
		$Ma = 0.78$ $\mathrm{Re} = 6.24\times10^6$ $\alpha = -0.9^\circ$	$C_{D4} \le C_{D4}^0$ $\lvert C_{m4}\rvert \le \lvert C_{m4}^0\rvert$
		$Ma = 0.80$ $\mathrm{Re} = 6.4\times10^6$ $\alpha = -0.9^\circ$	$C_{D5} \le C_{D5}^0$ $\lvert C_{m5}\rvert \le \lvert C_{m5}^0\rvert$
Hover flight $Ma = 0.6$ $C_L = 0.0$	$\lvert C_{m0}\rvert \le 0.01$	$Ma = 0.6$ $\mathrm{Re} = 4.8\times10^6$ $\alpha = -0.77^\circ$	$\lvert C_{m6}\rvert \le \lvert C_{m6}^0\rvert$
Maneuvering flight $Ma = 0.4$ $C_L = 0.0$	$\lvert C_{m0}\rvert \le 0.01$	$Ma = 0.4$ $\mathrm{Re} = 3.2\times10^6$ $\alpha = -0.75^\circ$	$\lvert C_{m7}\rvert \le \lvert C_{m7}^0\rvert$

In this paper, the in-house code PMB3D was employed for the flow field analysis. The steady RANS equations were solved using multi-block structured grids and the second-order Roe MUSCL scheme was used for spatial discretion. The SA turbulence mode was solved for turbulence simulation. The grid topology is C-type and the resolution is 449×73. Figure 9 is the grid distribution near the baseline airfoil for CFD simulations. The aerodynamic forces have been compared with the data from wind tunnel experiments. The simulations and experiments Ma=0.4, and Re = 1.4×10^6. Figure 10 shows the lift coefficients versus AoA and the Figure 11 shows the drag coefficients. The simulation results are in good agreement with the experiment.

The number of population is 54, and the objectives are solved in parallel on the high performance computer. The maximum iteration step is set to be 50. The NSGA-Ⅱ is also employed for comparison.

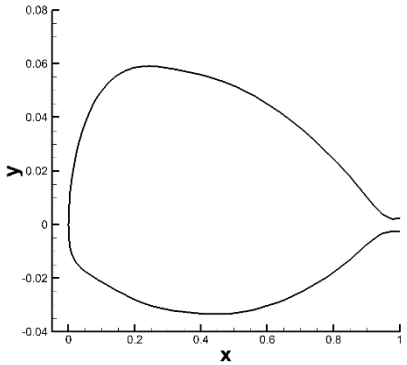

Figure 8 The OA209 airfoil

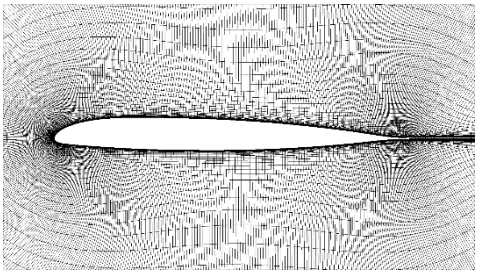

Figure 9 Schematic of computational grid

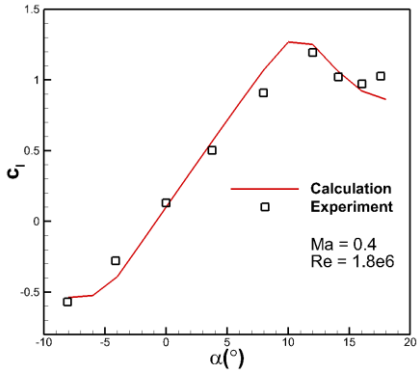

Figure 10 Comparison of lift coefficients between numerical results and experimental data

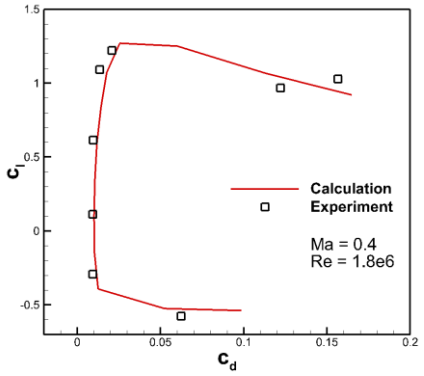

Figure 11 Comparison of drag coefficients between numerical results and experimental data

4.2 Results and analysis

The Pareto fronts obtained by the MR-EDA and NSGA-Ⅱ are presented in Figure 12~Figure 14. As we can see in the Figure 12, the first and second objective form a convex front, and the MR-EDA converges to a better front. The high performance of convergence is also indicated in Figure 13. A wider distribution of solution is generated by the MR-EDA. The fronts for the second and the third objective generated by the two methods are very close. We chose one optimal individual in the solution set obtained by the MR-EDA for a more detail analysis. The shape of the selected airfoil is shown in Figure 15.

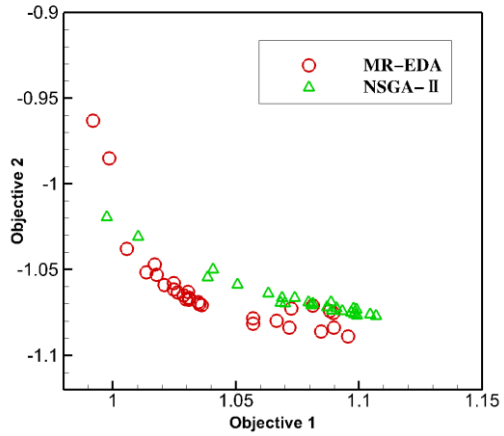

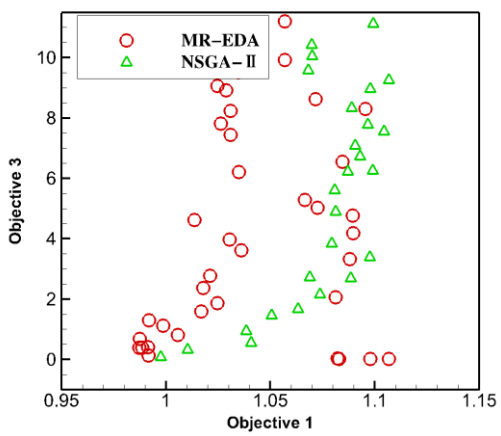

Figure 12 Optimal front obtained by the NSGA-Ⅱ and MR-EDA (Objective 1 vs. Objective 2)

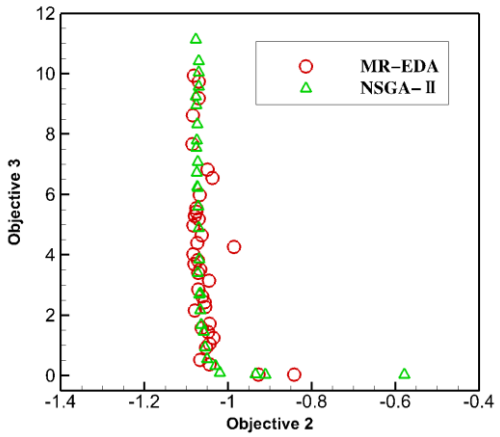

Figure 13 Optimal front obtained by the NSGA-Ⅱ and MR-EDA (Objective 1 vs. Objective 3)

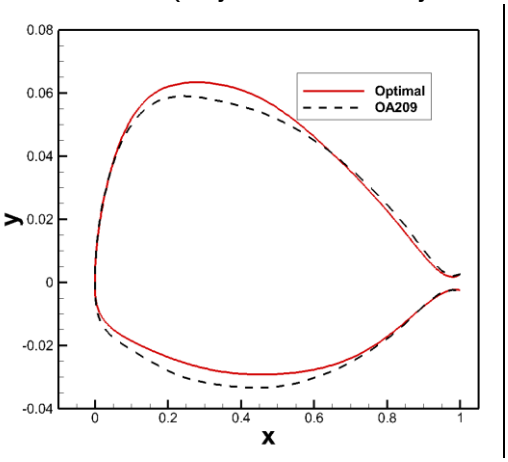

Figure 14 Optimal front obtained by the NSGA-Ⅱ and MR-EDA (Objective 2 vs. Objective 3)

Figure 15 Optimal airfoil by MR-EDA

Now we examine the aerodynamic performance of the optimal airfoil and compare with the baseline airfoil. Table 3 shows the airfoil performance at the first two design condition. The drag coefficient at $Ma = 0.6, C_L = 0.6$ is increased by 0.57%, which has a negligible change. For the maximum lift coefficient at $Ma = 0.4$, it increased by 3.76%.

The zero lift moment is critical for the operation performance. In the optimization problem, the moment is defined as constrains. In the Table 4, is shown the moment performance at 5 conditions. It obviously indicates that the level of moments of the optimal airfoil has been reduced significantly. For example, the moment coefficient at the hover flight is -4.4824×10^{-3} for the baseline airfoil and it is reduced to -0.2007×10^{-3} for the optimal airfoil.

The drag divergence performance is directly relative to the forward flight capability. It is defined as the third objective in the multi-objective optimization problem. Figure 16 is the curves of drag coefficients with the Ma number. As we can see in the figure, the drag divergence performance of the optimal airfoil is improved compared with the baseline airfoil.

In general, the overall performance of the rotor airfoil is improved using the MR-EDA. The maximum lift coefficient at maneuvering flight is increased by 3.76%, and the drag divergence performance is also improved. The zero lift moments are considered as constraints, and all the moments are improved significantly.

Table 3 Comparison of aerodynamic performance of the baseline and the optimized airfoil

Design Point	Objective	Baseline	Optimal	Δ (%)
Hover flight $Ma = 0.6$ $C_L = 0.6$	C_D	0.01044	0.0105	0.57%
Maneuvering flight $Ma = 0.4$ $C_L = C_{L\max}$	$C_{L\max}$	1.3499	1.4007	3.76%

Table 4 Zero lift moment coefficient at design point for the baseline and optimized airfoil

Design Point	Condition	Baseline ($\times10^{-3}$)	Optimal ($\times10^{-3}$)
Hover flight	$Ma = 0.6, \mathrm{Re} = 4.8\times10^6$	-4.4824	-0.2077
Maneuvering flight	$Ma = 0.4, \mathrm{Re} = 3.2\times10^6$	-3.8040	0.1419
Forward flight	$Ma = 0.76, \mathrm{Re} = 6.08\times10^6$	-6.5025	-1.8232
	$Ma = 0.78, \mathrm{Re} = 6.24\times10^6$	-7.0223	-2.3697
	$Ma = 0.80, \mathrm{Re} = 6.4\times10^6$	-8.2591	-5.3153

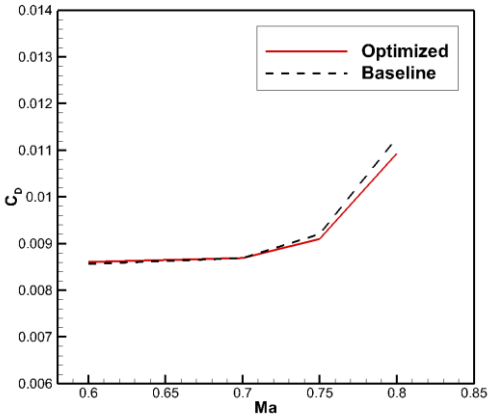

Figure 16 Drag coefficients with different Ma for the baseline and optimized airfoil ($\mathrm{Re} = Ma \times 8 \times 10^6, C_L = 0$)

5. Conclusion

This study addressed a multi-objective optimization for rotor airfoils employing the manifold learning method. The proposed methodology used the manifold information during the optimization process under the framework of estimation of distribution algorithms. The proposed methodology demonstrates that the optimization process converge rapidly and a Pareto optimal front has been obtained for the rotor airfoil design. The manifold leaning method has shown great prospect of application.

6. Contact Author Email Address

Song Chao: songchao@cardc.cn.

7. Copyright Statement

References

[1] Wang Q, Zhao Q, Wu Q. Aerodynamic shape optimization for alleviating dynamic stall characteristics of helicopter rotor airfoil[J]. Chinese Journal of Aeronautics, 2015, 28(2): 346-356.

[2] Hager J, Eyi S, LEE K. Multi-point design of transonic airfoils using optimization[C]//Guidance, Navigation and Control Conference. 1992: 4225.

[3] Jones B R, Crossley W A, Lyrintzis A S. Aerodynamic and aeroacoustic optimization of rotorcraft airfoils via a parallel genetic algorithm[J]. Journal of Aircraft, 2000, 37(6): 1088-1096.

[4] Massaro A, Benini E. Multi-objective optimization of helicopter airfoils using surrogate-assisted memetic algorithms[J]. Journal of Aircraft, 2012, 49(2): 375-383.

[5] Schutze O, Lara A, Coello C A C. On the influence of the number of objectives on the hardness of a multi-objective optimization problem[J]. IEEE Transactions on Evolutionary Computation, 2010, 15(4): 444-455.

[6] Zhao K, Gao Z, Huang J, et al. Aerodynamic optimization of rotor airfoil based on multi-layer hierarchical constraint method[J]. Chinese Journal of Aeronautics, 2016, 29(6): 1541-1552.

[7] Daskilewicz M J, German B J. Representing Sampled Pareto Frontiers as Parameterized Continuous Manifolds Using Self-Organizing Maps[J]. AIAA Journal, 2014, 52(11): 2480-2490.

[8] Yang D, Jiao L, Gong M, et al. Hybrid multi-objective estimation of distribution algorithm by local linear embedding and an immune inspired algorithm[C]//2009 IEEE Congress on Evolutionary Computation. IEEE, 2009: 463-470.

[9] Coello, C.A.C., Reyes Sierra, M.: A study of the parallelization of a coevolutionary multiobjective evolutionary algorithm. In: Monroy, R., Arroyo-Figueroa, G., Sucar, L.E., Sossa, H. (eds.) MICAI 2004. LNCS (LNAI), vol. 2972, pp. 688–697. Springer, Heidelberg (2004)

[10] H. Mühlenbein, G. Paa, From recombination of genes to the estimation of distributions I. B inary parameters, in: H.-M. Voigt, W. Ebeling, I. Rechenberger,H.-P. Schwefel (Eds.), roceedings of the Fourth International Conference onParallel Problem Solving from Nature (PPSN IV), vol. 114

of Lecture Notes inComputer Science, Springer, 1996, pp. 178–187.

[11] P. Larra˜ naga, J. Lozano (Eds.), Estimation of Distribution Algorithms: A New Tool for Evolutionary Computation, Kluwer Academic Publishers, Norwell, MA,USA, 2001.

[12] J. Lozano, P. Larra naga, I. Inza, E. Bengoetxea (Eds.), Towards a New evolutionary Computation: Advances on Estimation of Distribution Algorithms, vol. 192 of Studies in Fuzziness and Soft Computing, Springer, Secaucus, NJ, USA, 2006

[13]J. Friedman, T. Hastie, R. Tibshirani, Regularization paths for generalized linear models via coordinate descent, Journal of Statistical Software 33 (1) (2010) 1–22